Utilizing ultrasound as a surface digitization tool in image guided liver surgery

Kristen E. Miller[a], Janet E. Ondrake[a], Thomas S. Pheiffer[a], Amber L. Simpson[a], Michael I. Miga*[a,b,c]
[a]Department of Biomedical Engineering, Vanderbilt University, Nashville, TN, [b]Department of Radiology and Radiological Sciences, Vanderbilt University Medical Center, Nashville, TN, [c]Department of Neurological Surgery, Vanderbilt University Medical Center, Nashville, TN

*Michael.I.Miga@vanderbilt.edu; Phone: 615-343-8336; Web: http://bmlweb.vuse.vanderbilt.edu

ABSTRACT

Intraoperative ultrasound imaging is a commonly used modality for image guided surgery and can be used to monitor changes from pre-operative data in real time. Often a mapping of the liver surface is required to achieve image-to-physical alignment for image guided liver surgery. Laser range scans and tracked optical stylus instruments have both been utilized in the past to create an intraoperative representation of the organ surface. This paper proposes a method to digitize the organ surface utilizing tracked ultrasound and to evaluate a relatively simple correction technique. Surfaces are generated from point clouds obtained from the US transducer face itself during tracked movement. In addition, a surface generated from a laser range scan (LRS) was used as the gold standard for evaluating the accuracy of the US transducer swab surfaces. Two liver phantoms with varying stiffness were tested. The results reflected that the average deformation observed for a 60 second swab of the liver phantom was 3.7 ± 0.9 mm for the more rigid phantom and 4.6 ± 1.2 mm for the less rigid phantom. With respect to tissue targets below the surface, the average error in position due to ultrasound surface digitization was 3.5 ± 0.5 mm and 5.9 ± 0.9 mm for the stiffer and softer phantoms respectively. With the simple correction scheme, the surface error was reduced to 1.1 ± 0.8 mm and 1.7 ± 1.0 mm, respectively; and the subsurface target error was reduced to 2.0 ± 0.9 mm and 4.5 ± 1.8 mm, respectively. These results are encouraging and suggest that the ultrasound probe itself and the acquired images could serve as a comprehensive digitization approach for image guided liver surgery.

Keywords: image guided surgery, liver, ultrasound, registration, deformation

1. INTRODUCTION

Image guided procedures allow surgeons to apply data from pre-surgical images such as tumor location and vascular structure to the intra-operative physical space. This requires registration between pre-operative images and intra-operative data. For liver surgery, intra-operative surfaces have been obtained by various methods. Herline, et al. investigated the use of a tracked pen probe to digitize the surface of the liver for use in image guided liver surgery [1]. However, tracked pen probes are limiting because they provide sparse and often non-uniform data. Laser range scans have been effectively used to obtain intraoperative surface information during hepatic surgery, but involve introducing additional equipment into the OR [2]. Time-of-flight cameras are another modality that have been investigated for intraoperative surface data collection, but these cameras also take up addition space in the OR setting [3]. This excess equipment can be cumbersome to use and often introduces additional sterilization concerns. In this work, the use of an ultrasound transducer as a method of mapping the surface of the liver was investigated. While US swabbing is a contact method of surface mapping, this drawback could be outweighed by the efficiency in acquiring both surface and subsurface information simultaneously as well as being amenable to existing surgical workflow. That is, since intraoperative ultrasound already plays a large role in hepatic surgeries [4,5], US equipment is normally present in the OR during these procedures. Therefore, utilizing US to create a surface geometric representation of the liver could negate the need for additional imaging/digitization equipment in the OR. This paper aims to illustrate the possible use of US as a modality to map the surface of the organ intraoperatively, and discuss what measures can be taken to correct for the deformation caused by the US transducer compression itself during data collection.

2. METHODS

2.1 Tracking Calibration and Error Computation

Calibrating the position of the US transducer face was conducted by determining the location of four corner points on the US transducer face seen in Figure 1. These corners provided distinct markers that could be easily identified in the calibration process. An optically tracked pen probe was used to locate these four points in relation to the rigid body attached to the US transducer. This rigid body, which holds passive tracking spheres, was tracked using an NDI Polaris optical tracking system during the US swabbing. The calibration for the four corner points was then used to transform these points into the physical space of the swab.

The accuracy of this tracking was tested using a linear translating slide with millimeter accuracy. The US transducer was attached to the slide and moved specified distances ranging from 1 cm to 20 cm. The four corner points on the US transducer face were touched with the pen probe at the beginning and end of the movement, and the distance each of the points moved was calculated and compared to the actual distance the transducer had been moved on the slide.

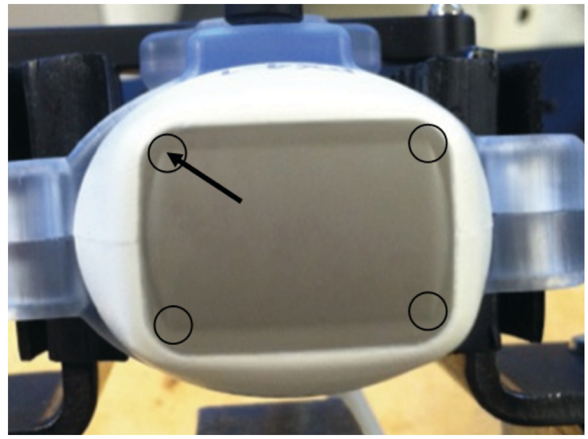

Figure 1: Four corner points on the face of the US transducer are circled, with an arrow indicating one of the points.

2.2 Data Acquisition

Ecoflex liver phantoms were used during the swabbing experiments (Figure 2). Trials were performed using two different phantoms with varied stiffness in order to investigate the efficacy of the technique on tissues-like phantoms with differing properties. Following the experimental trials, a section was removed and used for mechanical compression testing to determine the Young's Modulus of each phantom.

Trials using varying swab times of 40, 60 and 80 seconds were conducted to examine optimal surface coverage. In order to facilitate the calculation of the error associated with the US swab surfaces, a laser range scan was taken of the phantom before the US swabs were recorded.

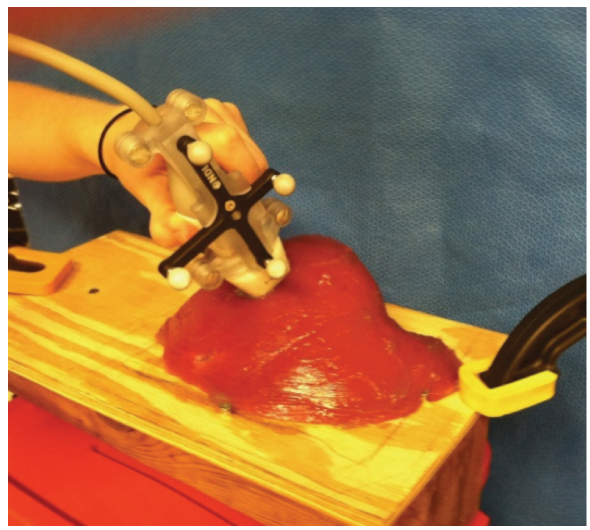

Figure 2: Set-up for tracked US swabbing.

2.3 Closest Point Distance Analysis

As a non-contact method to acquire surface data, the LRS was used as the gold standard for the intraoperative surface. The data associated with this gold standard was compared to our method of surface mapping using the US swabs. This assessment requires registering the LRS to a CT surface of the phantom using an iterative closest point rigid registration method [6], producing a LRS-to-CT registration (the ground truth physical-to-image registration in these experiments). The ultrasound swabs taken in physical space were then transformed using this transformation. The average closest point distance between the transformed LRS and US surfaces was then calculated to assess the digitization accuracy. If our technique was equivalent to the LRS gold standard, using the LRS-to-CT transformation on the US swab point cloud would produce an average closest point distance with an approximate zero mean.

2.4 Deformation Correction

Due to the contact nature of the method, a deformation correction was performed as an attempt to decrease the closest point distance error between the US surface swabs and the LRS surface gold standard. To correct for the deformation, points on the transformed US swab surface were projected out along their normals a distance equivalent to the average closest point distance calculated for all the trials of that phantom type. Then, a new US swab surface was created and closest point distances were calculated between this new surface and the LRS surface. These new average closest point distances were compared to the original average closest point distances to determine if the deformation correction decreased the error between the US swab surface and the gold standard LRS surface.

In addition, it is equally important to determine whether such a simple correction scheme may have deleterious effects on subsurface targets. To investigate this, ten subsurface targets were identified within the CT volume of each phantom for use in subsurface error calculations. The ground truth transformation was obtained from the CT-LRS registration. Each US swab surface was then registered to the CT volume, and these transformations were compared to the ground truth transformation. The target registration error (TRE) of the ten targets was computed for each trial.

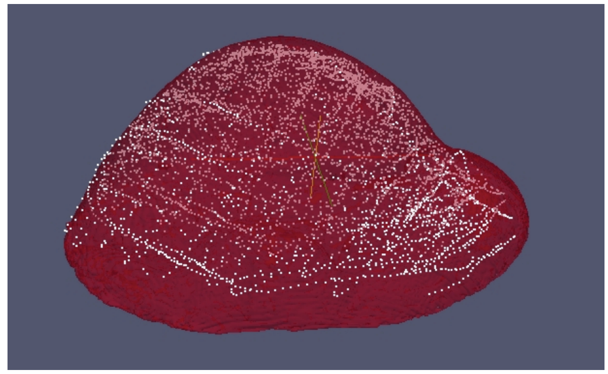

Figure 3: CT image surface (red) shown with point cloud from a sample US swab (white).

3. RESULTS

With respect to the calibration procedure test of verifying distances using a linear sliding translation scale, the error associated with tracking was within specifications of the optical tracking equipment as expected.

An example US swab point cloud is shown in Figure 3 along with the CT rendered liver surface. As expected, it was visually evident that US swab points lay below the CT surface due to the compression from the contact of the US transducer. Table 1 shows the average closest point distances calculated between the US swab surfaces and the CT surface for the nine time-varying trials for the stiffer phantom, while the average closest point distances calculated for the softer phantom trials are seen in Table 2. The mechanical testing of the phantoms determined that the Young's Modulus of the stiffer phantom and the softer phantom were approximately 17,000 Pa and 12,000 Pa respectively. A visual representation of the signed closest point distances for one of the uncorrected US swabs can be seen in Figure 4a.

	Length of Swab (s)	40	60	80
Avg. Closest Point Distance (mm)	Swab 1	3.4 ± 1.1	3.8 ± 1.0	3.6 ± 0.9
	Swab 2	3.6 ± 1.0	3.8 ± 1.0	3.9 ± 0.9
	Swab 3	4.1 ± 1.0	3.4 ± 1.0	3.8 ± 1.0
	Average	3.7 ± 1.0	3.7 ± 0.9	3.8 ± 0.9

Table 1. Average closest point distances between US swabs and LRS surfaces for stiffer phantom.

	Length of Swab (s)	40	60	80
Avg. Closest Point Distance (mm)	Swab 1	3.9 ± 1.6	4.9 ± 1.5	4.6 ± 1.4
	Swab 2	4.7 ± 1.3	4.2 ± 1.3	5.2 ± 1.1
	Swab 3	4.6 ± 1.8	4.8 ± 1.4	5.1 ± 1.3
	Average	4.4 ± 1.3	4.6 ± 1.2	5.0 ± 1.1

Table 2. Average closest point distances between US swabs and LRS surfaces for softer phantom

Observing Tables 1 and 2, it is clear that the softer phantom showed slightly greater average closest point distance results. This average deformation is most likely correlated to the decreased stiffness of the phantom resulting in greater deformation during swabbing. While the average closest point distances did not significantly vary over different time intervals, the 60 second swab time was determined to be optimal due to its ability to provide sufficient time for a distributed surface coverage with adequate overlap.

To compensate for deformation, the US swab points were projected an offset distance along the normal lines from the surface. The offset was estimated as the average closest point distance between the US surface and the LRS surface over all trials for the phantom. The average closest point distance for all of the softer phantom trials was 4.72 mm. The overall average closest point distance for the stiffer phantom trials was 4.24 mm. Tables 3 and 4 show the

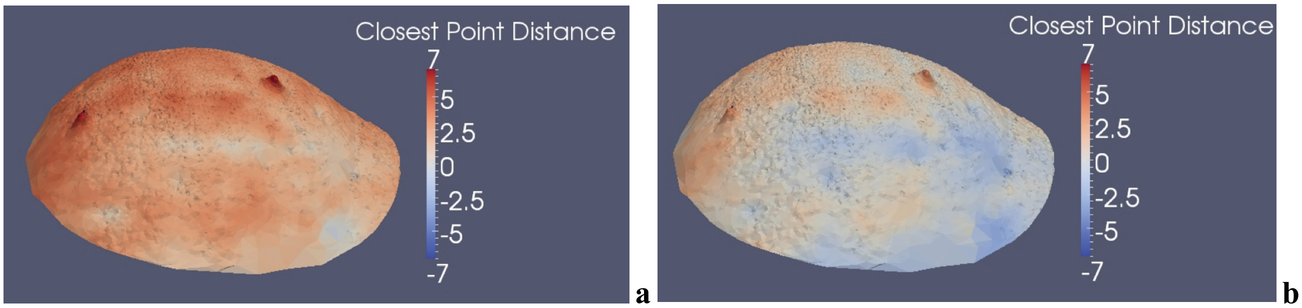

Figure 4: Closest point distances from LRS surface to a sample US swab, shown in mm, for (a) uncorrected US swab and (b) deformation corrected US swab.

average closest point distances between the corrected US surfaces and the LRS surfaces for the stiffer phantom and softer phantom respectively. Comparing these average closest point distances to those seen in the uncorrected US swab results in Tables 1 and 2, it is evident that the deformation correction significantly increased the accuracy of the US swab surfaces relative to the LRS gold standard. Figure 4b shows the closest point distances for a sample corrected US swab, with the white coloring representing a zero closest point distance between the two surfaces. The decrease in the average closest point distance from the uncorrected US surface seen in Figure 4a to the corrected US surface in Figure 4b is evident. The differing areas of red and blue coloring on the surface in Figure 4b reveal that some regions of the corrected US surface fall below the LRS surface, while others are now above the LRS. From this it can be deduced that the US swabbing is not applying even pressure in all regions of the liver, causing an

	Length of Swab (s)	40	60	80
Avg. Closest Point Distance (mm)	Swab 1	1.0 ± 0.8	1.2 ± 0.8	1.2 ± 0.9
	Swab 2	1.0 ± 0.7	1.2 ± 0.9	1.3 ± 0.8
	Swab 3	1.5 ± 0.9	0.9 ± 0.6	1.2 ± 0.9
	Average	1.2 ± 0.8	1.1 ± 0.8	1.2 ± 0.8

Table 3. Average closest point distances between corrected US swabs and LRS surfaces for stiffer phantom.

	Length of Swab (s)	40	60	80
Avg. Closest Point Distance (mm)	Swab 1	1.3 ± 1.0	2.0 ± 1.3	1.8 ± 1.2
	Swab 2	1.7 ± 1.0	1.3 ± 1.0	2.2 ± 0.9
	Swab 3	1.6 ± 1.4	1.9 ± 1.1	2.2 ± 1.1
	Average	1.5 ± 1.0	1.7 ± 1.0	2.1 ± 1.0

Table 4. Average closest point distances between corrected US swabs and LRS surfaces for softer phantom.

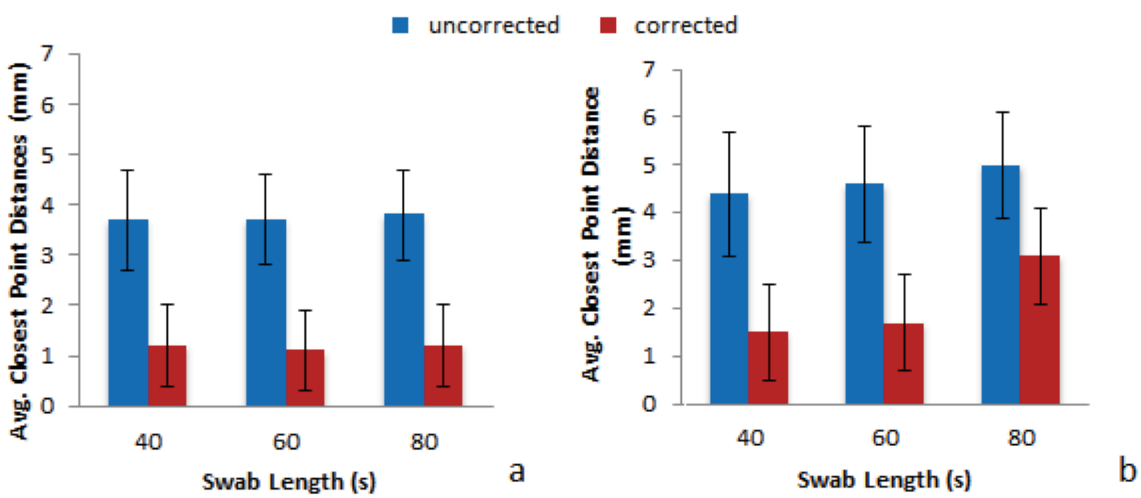

Figure 5. Average closest point distance for the varying swab lengths for (a) stiffer phantom and (b) softer phantom with and without correction.

uneven distribution of deformation. Figure 5 expresses the result of uncorrected and corrected closest point distance averaged over the entire surface for the different swabbing lengths with each respective phantom.

Figure 6 shows the 10 subsurface target locations in both phantoms, as well as the TRE values for the 10 targets for each swab, both with and without the deformation correction in place. The average TRE values for the stiffer phantom and softer phantom prior to correction were 3.5 ± 0.5 mm and 5.9 ± 0.9 mm respectively. Following deformation correction, the average TRE values were decreased to 2.0 ± 0.9 mm for the stiffer phantom and 4.5 ± 1.8 mm for the softer phantom. The TRE for the softer phantom targets were somewhat worse than those for the stiffer phantom. It is clear that the stiffer phantom is less impacted by the compression of swabbing. The greater TRE values for the softer phantom are most likely due to the greater compression of the phantom surface by the US transducer during data collection. Overall, the deformation correction applied to the US swabs decreased the TRE for the subsurface targets

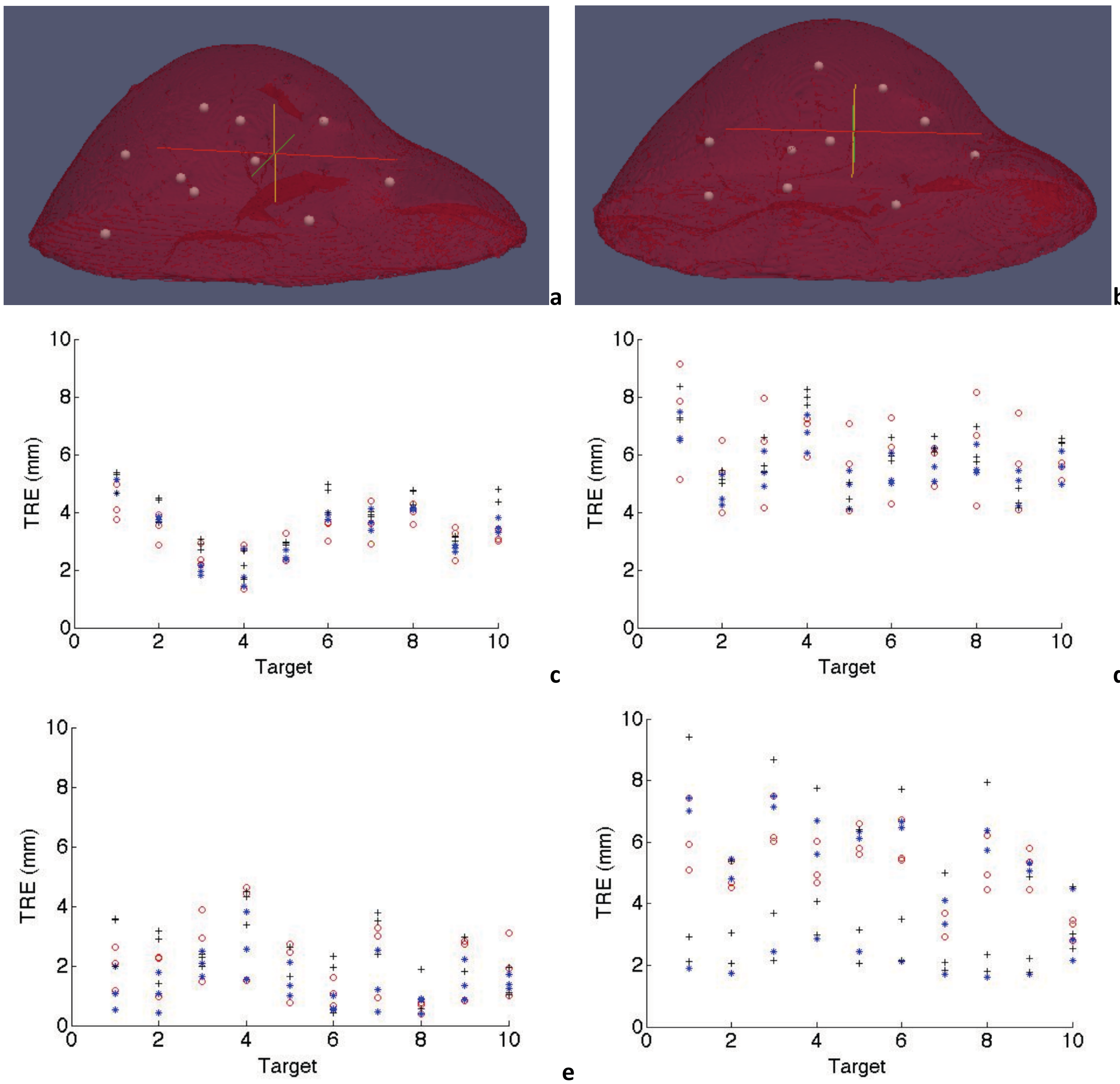

Figure 6. Ten subsurface targets within (a) stiffer and (b) softer phantoms. The TRE for the ten targets for the uncorrected US swabs for the (c) stiffer and (d) softer phantoms. The TRE for the ten targets for the corrected US swabs for the (e) stiffer and (f) softer phantom. Red circles are 40 second swabs, blue stars are 60 second swabs, and black pluses are 80 second swabs.

(Table 5). However, there was a greater variability in the effect of the deformation correction on TRE on the softer phantom as seen in Figure 6f.

	Stiff, Uncorrected			Stiff, Corrected			Soft, Uncorrected			Soft, Corrected		
Target	mean	min	max	mean	min	max	mean	min	max	mean	min	max
1	4.7 ± 0.5	3.8	5.4	2.0 ± 1.0	0.5	3.6	7.3 ± 1.2	5.1	9.1	5.5 ± 2.7	1.9	9.4
2	3.8 ± 0.5	2.9	4.9	1.8 ± 0.9	0.4	3.2	5.0 ± 0.7	4.0	6.5	4.1 ± 1.5	1.7	5.4
3	2.4 ± 0.5	1.8	3.1	2.4 ± 0.7	1.5	3.9	5.8 ± 1.1	4.1	8.0	5.7 ± 2.4	2.2	8.7
4	2.2 ± 0.6	1.4	2.9	3.4 ± 1.3	1.5	4.6	7.1 ± 0.8	5.9	8.2	5.1 ± 1.6	2.8	7.8
5	2.8 ± 0.4	2.3	3.3	1.9 ± 0.8	0.8	2.7	5.0 ± 1.0	4.1	7.1	4.9 ± 1.8	2.0	6.6
6	4.0 ± 0.6	3.0	5.0	1.1 ± 0.7	0.4	2.3	5.8 ± 0.9	4.3	7.3	5.1 ± 2.1	2.1	7.7
7	3.7 ± 0.4	2.9	4.4	2.3 ± 1.2	0.5	2.8	5.9 ± 0.6	4.9	6.6	3.1 ± 1.1	1.7	5.0
8	4.2 ± 0.4	3.6	4.8	0.9 ± 0.6	0.4	1.9	6.1 ± 1.1	4.2	8.2	4.6 ± 2.2	1.6	8.0
9	3.0 ± 0.4	2.3	3.5	2.0 ± 0.9	0.8	3.0	5.0 ± 1.1	4.1	7.4	4.1 ± 1.7	1.7	5.8
10	3.7 ± 0.6	3.0	4.8	1.6 ± 0.7	1.0	3.1	5.8 ± 0.6	5.0	6.6	3.2 ± 0.8	2.2	4.6

Table 5. Mean, minimum and maximum TRE values, in mm, for the ten targets for the uncorrected and corrected US swabs for stiff and soft phantoms.

4. DISCUSSION

Overall, the use of US technology to intraoperatively digitize the surface of the liver was found to be promising. The error associated with the mechanical pressure applied to the phantom organ during swabbing was significantly reduced by applying a deformation correction during data processing. Implementing a more sophisticated deformation correction algorithm could further compensate for the mechanical pressure error of the system. Observing the closest point distance between the US and LRS surfaces for the different trials revealed a trend in the magnitude of the deformation. There was a general finding that when swabbing anterior surfaces of the phantom, more deformation by the probe occurred when the corresponding posterior surfaces (surface directly below) had air gaps between the organ surface and the supportive platform (phantom did not sit flush with support). Implementing an organ support system that could accommodate this could additionally decrease deformation error. Fortunately, in the clinical scenario organ packing is often performed to stabilize the organ. An in vivo investigation will be in future work.

The deformation correction was shown to decrease the TRE associated with the subsurface targets identified in the phantoms. Although the TRE associated with each target was not decreased uniformly by the deformation correction, the efficacy of the deformation correction at decreasing the TRE did not appear to be linked with the depth of the target. The method pursued here is admittedly very simple; nevertheless, the results demonstrated an improvement and warrant further investigation with more sophisticated methods.

Since the phantom livers used in this experiment are not real human tissue, the results of the US surface swabbing technology with a human liver would vary from those achieved here. However, the approach here can translate quite easily for clinical testing, and the similar results across phantoms of varying stiffness does suggest that the clinical domain may be reflected reasonably well in these experiments. In the future, this method of mapping the surface could be combined with subsurface information as determined from segmenting ultrasound images to gain additional data.

5. CONCLUSION

This work discusses a novel use of US in image guided surgical procedures as a method for digitizing the surface of an organ intraoperatively. To our knowledge, this specific realization has not been explored in literature. The predominant focus in the literature has been at segmenting structures within the ultrasound images themselves to create surfaces [7,8,9,10,11] rather than using the probe itself as a swabbing stylus. The genesis of this work originated from the observation of surgical workflow during experimental image-guided liver surgery procedures. This application of

US would help decrease the additional devices in the OR currently required for image guided surgical procedures. This method of mapping intraoperative surfaces is fast and would not greatly interrupt the surgical procedure. Furthermore, the addition of a deformation correction process to account for the pressure applied to the surface by the US transducer could increase the accuracy of the surfaces obtained from the US swab data. Preliminary results from this study indicate that US technology may be an effective way to intraoperatively digitize the surface of the liver for image guided surgery purposes.

6. REFERENCES

[1] A.J. Herline, J.L. Herring, J.D. Stefansic, W.C. Chapman, R.L. Galloway, B.M. Dawant, "Surface registration for use in interactive image-guided liver surgery", Medical Image Computing and Computer-Assisted Intervention 1679, 892-899 (1999).

[2] L. W. Clements, W. C. Chapman, B. M. Dawant, R. L. Galloway, M. I. Miga, "Robust surface registration using salient anatomical features for image-guided liver surgery: Algorithm and validation", Medical Physics 35(6), 2528-2540 (2008).

[3] S. Bilings, A. Kapoor, M. Keil, B.J. Wood, E. Boctor, "A hybrid surface/image based approach to facilitate ultrasound/CT registration", Proceedings of SPIE 7968 (2011).

[4] J.M. Blackall, G.P. Penney, A.P. King, D.J. Hawkes, "Alignment of sparse freehand 3-D ultrasound with preoperative images of the liver using models of respiratory motion and deformation", IEEE Transactions on Medical Imaging 24(11), 1405-1416 (2005).

[5] M.D. Rifkin, F.E. Rosato, H.M. Branch, J. Foster, S.L. Yang, D.J. Barbot, G.J. Marks, "Intraoperative ultrasound of the liver", Annals of Surgery 205(5), 466-472 (1987).

[6] J.M. Fitzpatrick, M. Sonka, "Handbook of Medical Imaging, Volume 2. Medical Imaging Processing and Analysis" (2000).

[7] A. Ahmad, D. Cool, B.H. Chew, S.E. Pautler, T.M. Peters, "3D segmentation of kidney tumors for freehand 2D ultrasound", Proceedings of SPIE 6141, (2006).

[8] A. Ghanei, H. Soltanian-Zadeh, A. Ratkewicz, F.F. Yin, "A three-dimensional deformable model for segmentationn of human prostate from ultrasound images", Medical Physics 28(10), (2001).

[9] W.H. Nam, D.G. Kang, D. Lee, J.B. Ra, "Robust registration of 3-D ultrasound and CT images of the liver for image-guided intervention", IEEE International Symposium on Biomedical Imaging: From Nano to Macro, 1201-1204 (2010).

[10] P.C. Pederson, J.D. Quartararo, T.L. Szabo, "Segmentation of speckle-reduced 3D medical ultrasound images", Ultrasonics Symposium, 361-266 (2008).

[11] A.M. Kop, R. Hegadi, "Kidney segmentation from ultrasound images using gradient vector force", International Journal of Computer Application (2), 104-109 (2010).